Research Square

Preprints are preliminary reports that have not undergone peer review.
They should not be considered conclusive, used to inform clinical practice,
or referenced by the media as validated information.

Targeting HMGB1 Conformation with a Novel Antagonist: An Innovative Therapeutic Strategy to Inhibit HMGB1-Initiated Neuroinflammation in Epilepsy

Liaoxi Tan
China Pharmaceutical University
Xuewa Jiang
China Pharmaceutical University
Junyi Ye
China Pharmaceutical University
Weihang Yao
China Pharmaceutical University
Pingping Shen
Xuzhou College of Industrial Technology
Haixia Ge
Huzhou Normal University
Jian Zhang
1020071849@cpu.edu.cn

China Pharmaceutical University

Research Article

Keywords: HMGB1, Tetrahydroprotoberberine, Epilepsy, Neuroinflammation

Posted Date: October 28th, 2026

DOI: https://doi.org/10.21203/rs.3.rs-10771195/v1

License: This work is licensed under a Creative Commons Attribution 4.0 International License.
Read Full License

Additional Declarations: No competing interests reported.

Abstract

Epilepsy is a cerebral dysfunction disorder caused by aberrant hyperexcitability of neurons, and novel therapeutics targeting core epileptogenic mechanisms are urgently needed. Sustained neuroinflammation accumulates post-seizure in epileptic foci, which further drives recurrent seizures. High-mobility group box 1 (HMGB1), a vital damage-associated molecular pattern (DAMP), mediates the initiation and progression of epileptogenic inflammation. Therefore, we propose a novel anti-epileptic strategy: modulating the spatial conformation of HMGB1 to block the pro-inflammatory function and alleviate secondary inflammatory injury to epileptic lesions. To validate this strategy, GP10, a tetrahydroprotoberberine (THPB) derivative selectively suppressing HMGB1 pro-inflammatory activity, was utilized as a tool compound to interfere with HMGB1-triggered neuroinflammation. Mechanistically, GP10 specifically bound to phenylalanine 89 and induced conformational changes in HMGB1, which underpinned the selective suppression by GP10 of HMGB1-triggered inflammatory cascades at the cellular level. In the pilocarpine-induced mouse epilepsy model, GP10 markedly attenuated neuronal loss and neuroinflammation triggered by neuronal hyperexcitability, thereby alleviating secondary recurrent seizures. Collectively, this study demonstrated that targeting HMGB1-initiated inflammatory signaling is an effective strategy to ameliorate and retard epileptic seizures, providing novel mechanistic insights for discovering natural anti-epileptic drugs.

Highlights

1. Selective intervention of the HMGB1-mediated neuroinflammatory pathway represents a novel strategy for epilepsy treatment.
2. This study identified a novel THPB derivative GP10 that selectively suppresses HMGB1-induced neuroinflammation.
3. GP10 modulate HMGB1 conformation to suppress HMGB1-TLR4/RAGE-mediated pro-inflammatory signaling.
4. GP10 markedly ameliorates neuronal loss, neuroinflammation, and secondary seizure in epileptic mice at low doses.

Introduction

Epilepsy is a chronic brain disorder characterized by abnormal neuronal discharges and recurrent seizures. Conventional clinical antiepileptic drugs only alleviate seizure symptoms without modulating the fundamental pathogenic mechanisms, and cause severe side effects such as dizziness and cognitive dysfunction (Jehi 2025; Krishnamurthy. and B. 2025). Thus, novel therapeutic drugs and strategies targeting pathogenesis of epilepsy are urgently required.

Recent studies indicate that epileptic seizures are accompanied by neuroinflammatory cascades (Ava. and R. 2024; Grote et al. 2023; Ravizza et al. 2024). Within this pathological microenvironment, injured neurons-secreted damage-associated molecular patterns (DAMPs) were recognized by pattern

recognition receptors (PRRs) on infiltrating glia. This interaction triggers innate immune responses, worsening lesions, reducing seizure thresholds and inducing relapse (Brennan et al. 2021; Eberhard et al. 2024; Ravizza et al. 2018). High mobility group box 1 (HMGB1), a prototypical DAMP, is highly accumulated in epileptic foci (Zurolo et al. 2011). By binding to toll-like receptor 4 (TLR4) and the receptor for advanced glycation end products (RAGE), HMGB1 promotes glial activation, mediates inflammatory storms, and blood-brain barrier (BBB) disruption (Brennan, Garcia-Curran, Patterson, Luo and Baram 2021; Shi et al. 2018; Xie et al. 2017). HMGB1-targeted neutralizing antibodies and inhibitors relieve seizures in animal models (Lim et al. 2025; Wang et al. 2023; Wei et al. 2025). Yet these approaches hinder long-term chronic therapy, with limits including high required doses, disrupted physiological repair of HMGB1 due to pan-inhibition, and prohibitive medical costs.

Tetrahydroprotoberberines (THPBs), active constituents from *Corydalis yanhusuo* and *Stephania* plants, possess favorable BBB permeability and relieve central nervous system (CNS) disorders via dopamine signaling modulation (Bu et al. 2022; Zheng et al. 2018). While research on THPBs for epilepsy remains scarce, preliminary studies demonstrate their specific binding to the HMGB1 A-box domain and inhibition of HMGB1-mediated inflammation (Nesbit et al. 2024; Nesbit and Phillips 2020). Accordingly, this study aims to develop a novel therapeutic strategy for epilepsy by screening small molecules that specifically bind HMGB1 and modulate its spatial conformation, suppressing neuroinflammation induced by HMGB1 as a DAMP, thereby mitigating recurrent seizures.

Thus, by measuring compound inhibition of HMGB1- and lipopolysaccharide (LPS)-induced inflammation, we identified GP10 as a selective HMGB1 modulator from 27 THPBs synthesized from berberine and palmatine (Ge et al. 2021). Notably, GP10 significantly inhibited HMGB1-induced microglial inflammatory responses, while exerting minimal effects on LPS-induced inflammation. Multi-spectroscopic data validated that binding of GP10 to the HMGB1 B-box triggers conformational changes in HMGB1. Using molecular docking and site-directed mutagenesis, we identified phenylalanine (Phe) 89 as the key binding site for the interaction of GP10 with HMGB1. In a pilocarpine-induced mouse model of epilepsy, compared with glycyrrhizin, GP10 markedly attenuated epilepsy-associated hippocampal neuronal loss and inflammatory storm, and significantly alleviated secondary seizure at low doses. These findings highlight the feasibility of disrupting HMGB1-mediated signaling via conformational modulation, offering a promising strategy to mitigate post-seizure inflammatory damage in epileptic foci and alleviate recurrent seizures.

Materials and methods

Cell culture and treatment

BV2 cells were obtained from the Chinese Academy of Sciences and cultured in Dulbecco's modified eagle medium (DMEM, Gibco.) supplemented with 10% fetal bovine serum (FBS, Gibco.) and 1% penicillin-streptomycin (P/S, NCM Biotech.). Passaging was performed when cell confluence reached

70–80%. The cells were maintained in a humidified incubator (Thermo Fisher Scientific.) at 37 ℃ with 5% CO_2.

For efficacy experiments, cells were divided into vehicle, model, and treatment groups. Prior to drug administration, 5 μg/mL purified HMGB1 or 1 μg/mL LPS (Sigma.) was thoroughly mixed with the test compound in serum-free DMEM and pre-incubated at 4 ℃ for 24 h. For the model group, 0.1% dimethyl sulfoxide (DMSO, Solarbio.) in serum-free DMEM was pre-incubated. Concurrently, cells were seeded at an appropriate density into cell culture plates and cultured for 24 h to achieve stable conditions.The cell culture supernatant in the plates was replaced with serum-free medium, and cells were subjected to starvation in the incubator for 1 h. Cells were treated for 3 h for subsequent RNA and protein extraction, or fixed for immunofluorescence. Cell culture supernatants were harvested after 12 h incubation for quantification of inflammatory cytokine release, whereas NO production in supernatants was assessed at 24 h after incubation.

Purification of HMGB1-full length, HMGB1 A-box, and HMGB1 B-box

Plasmids containing HMGB1 full-length, HMGB1 A-box, and HMGB1 B-box genes were transformed into competent *Escherichia coli.* (*E. coli*) BL21(DE3). Positive BL21(DE3) clones were cultured overnight in 20 mL Luria-Bertani (LB) medium with 50 μg/mL kanamycin at 37 ℃ and 220 rpm. Expanded cultured BL21(DE3) cells were grown to an optical density $(OD)_{600}$ of 0.6–0.8 and induced with 0.5 mM Isopropyl-β-D-thiogalactopyranoside (IPTG, Biosharp.). After overnight incubation at 18 ℃, the cells were harvested via centrifugation at 8000 rpm for 10 mins at 4 ℃, then the bacterial pellet was resuspended in Tris buffered saline (TBS, pH 7.4) and lysed with TieChui™ *E.coli* lysis buffer (ACE Biotechnology.) for 10 mins, and unlysed debris was removed by centrifugation at 12000 rpm for 20 mins at 4 ℃ to collect the supernatant. The supernatant was applied to a pre-equilibrated Ni^{2+}-NTA agarose column, which was washed with wash buffer before recombinant proteins were eluted with elution buffer. For further purification of full-length HMGB1, the eluted protein was dialyzed overnight at 4 ℃ against buffer A (20 mM sodium phosphate monobasic, pH 7.4), then loaded onto a pre-equilibrated 5 mL HiTrap Q column (equilibrated with buffer A). The column was washed with 5 column volumes of buffer A, and bound proteins were eluted with a linear salt gradient (0.1–0.5 M NaCl) at a flow rate of 1 mL/min, with 2.5 mL fractions collected. Finally, the purified proteins were passed through a polymyxin B column (Genscript.) to remove contaminating lipopolysaccharide, and protein purity was assessed by SDS-PAGE and Coomassie Brilliant Blue R-250 staining (Beyotime.). Approximately 6 mg of HMGB1 protein was obtained per liter of bacterial culture.

Animal and epilepsy model establishment

The pilocarpine-induced mouse model was established according to previous literature (Balaha et al. 2023; Guo et al. 2022). To ensure a survival rate, this experiment modified the dose and injection frequency of pilocarpine. Briefly, 180 mg/kg lithium chloride was injected intraperitoneally. After 18–20 h,

1 mg/kg atropine sulfate was injected intraperitoneally. After 20 mins, 230 mg/kg pilocarpine hydrochloride was injected, and then 100 mg/kg pilocarpine hydrochloride was injected every 30 mins until the seizure severity of the mice reached or exceeded Racine score IV (Grade I: rhythmic mouth or facial twitching; Grade II: head nodding or tail flicking; Grade III: unilateral limb twitching; Grade IV: multiple limb twitching or rigidity; Grade V: generalized tonic-clonic seizure), and the seizure duration exceeded half an hour. Control group mice were injected with an equal volume of normal saline (n = 8 per group). After model establishment, Upon successful model induction, mice with comparable Racine scores were randomly assigned to five groups: model group, 1 mg/kg GP10, 3 mg/kg GP10, 10 mg/kg GP10, and 100 mg/kg glycyrrhizin group (n = 8 per group). To investigate the therapeutic effect of the drugs on the epilepsy model, three concentrations of GP10 and glycyrrhizin were intraperitoneally injected into mice in each group 3 h after the first model establishment, subsequently for 3 days, and 1 h before the second model establishment. The control group and model group were given an equal volume of normal saline. After 3 days of drug administration, a second model was established using the same method as the first time. Drug administration was concluded when the Racine scores of all mice in the model group reached or exceeded Racine score grade IV, and the Racine scores of each group were recorded. Hippocampal tissue and venous blood were collected 3 h after drug administration.

Male mice aged 6–8 weeks were purchased from Annocare Biotechnology and housed in an SPF-grade animal experimental center under a 12 h light-dark cycle at 23 ± 2 ℃ for 72 h of acclimatization prior to experiments.

Hematoxylin-eosin (HE) & nissel staining

The mouse hippocampus tissue was fixed with 4% paraformaldehyde prepared with physiological saline for 24–48 h, and then embedded, sectioned, stained, and scanned by Nanjing Frays Bio-Technology. ImageJ was used to count the number of neurons in each region of the hippocampus tissue.

Enzyme-linked immunosorbnent Assay (ELISA).

According to the Mouse TNF-α (Tumor Necrosis Factor Alpha) ELISA Kit (Elabscience.) determination method, the cell culture supernatant was diluted and the content of TNF-α in the supernatant was detected. According to the Mouse High mobility group protein B1, HMGB-1 ELISA Kit (CUSABIO) determination method, the mouse serum was diluted and the content of HMGB1 in the serum was detected.

Nitric oxide (NO) production measurement

Prior to cell stimulation, GP10 at concentrations of 0.3 μM, 1 μM and 3 μM was pre-incubated with 5 μg/mL HMGB1 or 1 μg/mL LPS for 24 h. Following 24 h of cellular stimulation, culture supernatants were harvested. The Griess reagent kit (Beyotime, Cat. No. S0023) was used to measure the NO levels at 540 nm. NO concentrations were calculated according to the standard curve generated using sodium nitrite.

RNA extraction and quantitative reverse transcription polymerase chain reaction (qRT-PCR) assay

Total RNA was isolated and purified from mouse hippocampal tissue or cultured cells using RNAiso Plus (Takara) and subsequently reverse transcribed into cDNA fragments using HiScript IV 1st Strand cDNA Synthesis Kit (+ gDNA wiper, Vazyme.). qRT-PCR was performed on a MA-6000 Real-Time Quantitative Thermal Cycler Molarray.) using 2× SYBR Green qPCR Master Mix (Selleck.). Relative expression levels of the target gene were normalized against the internal control *glyceraldehyde – 3-phosphate dehydrogenase* (*Gapdh*) and quantified using the $2^{-\Delta\Delta Ct}$ method. The primer sequences used are as follows: mouse *Gapdh* forward primer: CATCTTCCAGGAGCGAGACC. mouse *Gapdh* reverse primer: GAAGGGGCGGAGATGATGAC. mouse *interleukin (Il)-1β* forward primer: GAAATGCCACCTTTTGACAGTG. mouse *Il-1β* reverse primer: TGGATGCTCTCATCAGGACAG. mouse *Il-6* forward primer: GAGGATACCACTCCCAACAGACC. mouse *Il-6* reverse primer: AAGTGCATCATCGTTGTTCATACA. mouse *Tnf-α* forward primer: GCGACGTGGAACTGGCAGAAG. mouse *Tnf-α* reverse primer: GCCACAAGCAGGAATGAGAAGAGG. mouse *inducible nitric oxide synthase* (*Inos)* forward primer: GAGACAGGGAAGTCTGAAGCAC. mouse *Inos* reverse primer: CCAGCAGTAGTTGCTCCTCTTC. mouse *heme oxygenase 1* (*Ho-1)* forward primer: AAGCCGAGAATGCTGAGTTCA. mouse *Ho-1* reverse primer: GCCGTGTAGATATGGTACAAGGA. mouse *Hmgb1* forward primer:GGCGAGCATCCTGGCTTATC. mouse *Hmgb1* reverse primer: GGCTGCTTGTCATCTGCTG. To analyze mRNA expression, the data were standardized with the control group as the reference to reduce variance.

Protein extraction and Western Blotting (WB) Assay

Total protein was extracted from mouse hippocampal tissue or cultured cells using RIPA lysis buffer (supplemented with PMSF and phosphatase inhibitors, Beyotime.). Protein concentration was determined via an enhanced BCA protein assay kit (Beyotime.). After adding 5× SDS-PAGE loading buffer, samples were boiled for protein denaturation. Gels were prepared with the Omni-Easy™ One-Step PAGE Gel Fast Preparation Kit (Epizyme Biotech.). Electrophoresis was performed at 80 V for 20 min, then 120 V until proteins reached the gel edge. Membrane transfer was conducted at low temperature for 2 h under 220 mA constant current. Membranes were blocked with QuickBlock™ Blocking Buffer (Beyotime.) for 1 h, washed with TBS-Tween (TBST), and incubated with primary antibody overnight at 4 ℃. The primary antibodies used in this study include β-tubulin antibody (1:10000), β-actin antibody (1:10000), IL-1β antibody (1:2000), NOD-like receptor thermal protein domain-associated protein 3 (NLRP3) antibody (1:5000) and HO-1/HMOX1 antibody (1:3000) from Proteintech; Phospho (p)-nuclear factor-κB (NF-κB) antibody (1:2000), NF-κB antibody (1:2000), p-p38 mitogen-activated protein kinase (MAPK) antibody (1:2000), p38 MAPK antibody (1:2000), p-extracellular regulated protein kinases (ERK) antibody (1:2000), ERK antibody (1:2000) from Cell signaling technology. Following another TBST wash, membranes were incubated with secondary antibody (1:2000, Cell signaling technology.) for 1 h at room temperature. Band images were acquired and grayscale values quantified using a ChemiDoc™ imaging system (Bio-

Rad.) after incubation with ECL chemiluminescent substrate (ultra-sensitive, Biosharp.). Grayscale intensity of protein bands in each group was normalized to internal reference proteins, and data were standardized against the control group to reduce variability.

Methyl thiazolyl tetrazolium (MTT) cytotoxicity assay

BV2 cells were seeded in 96-well plates at 15,000 cells/well. After 24 h of adhesion, different concentrations of test drugs were added, followed by another 24 h of incubation. 100 μL of 5 mg/mL MTT was added to each well, and cells were incubated at 37 ℃ for 1 h-microscopic observation confirmed purple crystals in most cells. The supernatant was removed, and 150 μL of DMSO was added per well. After 10 mins of shaking in a microplate reader, absorbance was measured at 570 nm with a reference wavelength of 650 nm. Absorbance values of each group were corrected against the control group.

Immunocytofluorescent assay

After drug treatment of BV2 cells, culture medium was aspirated. Cells were washed three times with phosphate buffered saline (PBS), fixed with ice-cold methanol at -20 ℃ for 10 mins, then washed three times with PBS again. Following PBS removal, cells were blocked with 5% Bovine serum albumin (BSA) for 1 h. Blocking solution was discarded, and the same volume of NF-κB antibody (1:400, Cell signaling technology.) was added for overnight incubation at 4 ℃. Primary antibody was removed, and cells were washed three times with PBS before adding species-specific secondary antibody. Incubation was performed for 1 h at room temperature in the dark. After secondary antibody removal and three additional PBS washes, 50 μL Antifade Mounting Medium with Hoechst 33342 (Beyotime.) was edded to each well. Images were captured using a Leica fluorescence microscope. The percentage of positive cells was calculated as: (number of positively stained cells / total cell count) × 100%.

Surface plasmon resonance (SPR) assay

The process of immobilizing the protein is consistent with previous studies (Meng et al. 2025). Finally, the immobilization level of HMGB1 reached 7000 response units (RU). Binding experiments were performed at 25 ℃, and PBS-P+ (Cytiva.) with 5% DMSO was used as the running buffer. GP10 (0.78–100 μM) was continuously injected into the HMGB1-coated chip surface at a flow rate of 30 μL/min for 60 s, followed by dissociation in the running buffer for 60 s to evaluate its binding efficacy to HMGB1. The collected sensorgrams were analyzed using Biacore S200 Evaluation 3.0 software, and nonlinear fitting was performed using a 1:1 steady-state binding isotherm model to obtain the binding constant K_D.

Ultraviolet (UV) spectroscopy assay

Take quartz cuvettes, add HMGB1 at 3 μM and GP10 at different concentration ranges respectively. Using buffer solution (PBS, pH = 7.4) as reference, record the UV-visible absorption spectrum of the

reference solution in the wavelength range of 200–400 nm with a signal collection interval of 1 nm to eliminate the influence of the buffer's UV absorption.

Steady-state fluorescence spectroscopy assay

Take a quartz cuvette, add HMGB1 (3 μM), then sequentially add GP10 to final concentrations of 0-100 μM, and incubate for 5 mins. The sample without the compound served as the negative control. Measure the steady-state fluorescence spectrum in the range of 290–400 nm at 25 ℃, with excitation wavelength of 273 nm, excitation and emission slit widths of 10 nm each, and scan rate of 1200 nm/min.

Circular dichroism (CD) Assay

HMGB1 at a final concentration of 3 μM was sequentially added to GP10 solutions with final concentrations 50 μM. After a 5 mins incubation, the mixtures were placed in a quartz absorption cell. CD spectra of the samples were scanned over the range of 195–260 nm, with a step size of 1 nm and a scanning speed of 200 nm/min. The PBS served as the negative control.

Particle size and thermal stability determination

HMGB1 protein solution (1 mg/mL) was incubated with 200 μM GP10 for 5 min, with a ligand-free blank control group set in parallel. Samples were detected using Prometheus Panta NT.48 nano differential scanning fluorimeter. Standard-grade glass capillaries were filled with 40 μL of the sample, excitation light was preadjusted to get fluorescence readings above 2000 arbitrary units for F_{330} and $F_{350,}$ and samples were measured in temperature range 25–95 ℃ with temperature slope of 1 ℃/min. Up to 48 samples could be measured simultaneously. Prior to the measurements samples were centrifuged for 10 min at 16000 g at 4 ℃ to remove any large aggregates.

Molecular docking

The chemical structure of the small molecule was drawn using ChembioDraw 2012 software, and its 2D structure was converted to 3D via Chem3D. Energy minimization was performed using the MM2 method, and the structure was saved as a mol file. The 3D structures of HMGB1 were downloaded from the Protein Data Bank (http://www.pdb.org) for later use (HMGB1: 2yrq).The above structures were imported into the drug molecular design software Schrödinger separately. The LigPrep module was used to process the small molecule, generating different protonation states and stereoisomers. The Protein Preparation Wizard module was applied to optimize the target protein, obtaining the initial conformation before docking. The Receptor Grid Generation module was used to define the binding site on the protein surface (referring to literature reports) and generate a grid file. Finally, the GlideXP docking program was used, with other parameters set to the default values of Schrödinger. Docking results were evaluated using the scoring function built into Schrödinger. From the multiple conformations generated for GP10, the one with the highest score was selected for analysis to determine the type of interaction forces, binding distance, and potential number of binding sites.

Site directed mutagenesis

The site-directed mutagenesis primers were designed using the Vazyme primer design tool, and the primer sequences were as follows: *Hmgb1-K88A* forward primer: AAGCATTCAAAGACCCGAACGCTCCGAAACGT. *Hmgb1-K88A* reverse primer: CGGGTCTTTGAATGCTTTTTTGGTTTCACCTTTCGGC. *Hmgb1-F89A* forward primer: AAAAAGCCAAAGACCCGAACGCTCCGAAACGT. *Hmgb1-F89A* reverse primer: CGGGTCTTTGGCTTTTTTTTTGGTTTCACCTTTCG. PCR amplification were generated using 2 × KeyPo Master Mix (Dye Plus) from Vazyme. PCR products were digested with Dpn to remove unreacted template plasmids, then transformed into *E. coli* and inversely cultured at 37℃ overnight on LB solid medium. Single colonies were selected for expansion, and site-directed mutagenesis was verified by sequencing. Purification was performed according to the aforementioned protein purification method to obtain the corresponding mutant proteins.

Statistical analysis

Data were analyzed and graphed using GraphPad Prism 6.0 software (Resource Number: SCR_002798; Institution: GraphPad Software, Inc.; Address: San Diego, California, USA). All data are presented as mean ± standard error of the mean (SEM). Statistical significance was determined using unpaired Student's t-test or one-way analysis of variance (ANOVA). A *P*-value < 0.05 was considered statistically significant. All data were tested for normal distribution and equal variance.

Results

GP10 was identified as a candidate drug for selective HMGB1 inhibition

Figure 1 Screening THPBs that selectively suppress HMGB1 pro-inflammatory activity. (**a**) The skeleton of THPBs. (**b**) Inhibition rate of GPs on TNF-α release from BV2 cells induced by 5 μg/mL HMGB1 or 1 μg/mL LPS for 12 h. (**c**) Inhibition rate of Gs on TNF-α release from BV2 cells induced by 5 μg/mL HMGB1 or 1 μg/mL LPS for 12 h. All bar graphs represent mean ± SEM, n = 3.

with > 50% inhibition on HMGB1-induced inflammation for their effects on LPS- stimulated TNF-α release in BV2 cells, to exclude direct TLR4/RAGE inhibition and confirm HMGB1 selectivity (Feng et al. 2024; Luo et al. 2025; Özbay Kurt et al. 2024). The structures of THPBs, along with their respective inhibition rates on TNF-α release from HMGB1- and LPS-stimulated BV2 cells, are compiled in Table. S1-2.

Based on these results, GP9, GP10, and GP12 were identified as candidate compounds (Fig. 1b-c). Given that GP10 exhibited the most potent and selective inhibition of HMGB1-mediated pro-inflammatory activity, further investigations were conducted to elucidate the underlying mechanisms of GP10's *in vitro* efficacy and *in vivo* pharmacological activities in animal models.

GP10 selectively inhibited HMGB1-induced BV2 inflammation

First, we investigated the effect of GP10 on BV2 cell viability. As shown in Fig. 2b, GP10 exhibited minimal toxicity to BV2 cells at a maximum concentration of 30 μM, suggesting that GP10 possesses a good safety profile. Subsequently, replicate experiments (Fig. 2c) demonstrated that at a concentration of 10 μM, GP10 significantly reduced 5 μg/mL HMGB1-induced TNF-α release ($p < 0.01$), while having no significant effect on 1 μg/mL LPS-induced TNF-α release. To ensure the selectivity of GP10 for HMGB1, we selected 3 μM as the effective concentration for further investigation.

As shown in Fig. 2d, 3 μM GP10 significantly inhibited NO release from HMGB1-stimulated BV2 cells ($p < 0.0001$), whereas GP10 exerted no obvious effect on LPS-induced NO production. Meanwhile, Fig. 2e-h demonstrated that 3 μM GP10 significantly attenuated the HMGB1-induced upregulation of *Il-1β* ($p < 0.0001$), *Il-6* ($p < 0.0001$), *Tnf-α* ($p < 0.0001$), and *Inos* ($p < 0.001$) mRNA expression. However, 3 μM GP10 failed to reverse the LPS-induced upregulation of *Il-1β*, *Il-6*, *Tnf-α*, and *Inos* mRNA in BV2 cells, suggesting that GP10 selectively acts on HMGB1 signaling to modulate inflammatory mediator expression. In parallel, the concentration-dependent inhibition of HMGB1 signaling by GP10 was also assessed. As depicted in Fig. 2i-m, GP10 was found to inhibit HMGB1-induced BV2 inflammatory effects in a concentration-dependent manner across concentrations of 0.3 μM, 1 μM, and 3 μM. Specifically, 0.3 μM GP10 significantly suppressed HMGB1-induced upregulation of NO release ($p < 0.0001$) and mRNA expression for *Il-1β* ($p < 0.01$), *Il-6* ($p < 0.001$), *Tnf-α* ($p < 0.05$), and *Inos* ($p < 0.01$). These findings suggest that GP10 can effectively block HMGB1-induced inflammation even at a lower concentration.

GP10 selectively inhibited HMGB1-induced inflammatory-related signaling pathways activation

HMGB1 exerts pro-inflammatory activity via two classic pathways, NF-κB and MAPK (Ma et al. 2025; Ye et al. 2023). Results in Fig. 3a-e showed that HMGB1 significantly upregulated NLRP3 expression and increased p38, ERK, and NF-κB phosphorylation ($p < 0.0001$), confirming the activation of cellular inflammatory pathways. In BV2 cells, GP10 at 0.3 μM, 1 μM, and 3 μM concentration-dependently attenuated HMGB1-induced upregulation of NLRP3 expression as well as phosphorylation of NF-κB, p38, and ERK ($p < 0.05$), with 3 μM GP10 significantly inhibiting the activation of the HMGB1-induced inflammatory pathway ($p < 0.01$). However, Fig. 3f-j revealed that under the same stimulation conditions, 3 μM GP10 had no significant effect on LPS-induced upregulation of NLRP3 expression, p38 phosphorylation, ERK phosphorylation and NF-κB phosphorylation, further confirming its selectivity for HMGB1 signaling.

NF-κB nuclear translocation is an early event in NF-κB pathway activation that positively regulates pro-inflammatory factor expression and release (Park et al. 2017). As shown in Fig. 3k-l, cellular immunofluorescence analysis showed HMGB1 stimulation of BV2 cells for 3 h induced significant NF-κB nuclear localization ($p < 0.0001$), while 3 μM GP10 significantly attenuated NF-κB nuclear localization ($p < 0.001$). In summary, GP10 effectively alleviates HMGB1-induced inflammatory effects, characterized by low concentrations and high selectivity toward HMGB1-induced effects.

GP10 bound HMGB1 and thereby induced its conformational changes

Given the selectivity of GP10 for HMGB1 signaling, the binding characteristics in regulating HMGB1-mediated inflammation was investigated. SPR was employed to assess the HMGB1-GP10 interaction. Under 60 s association-dissociation conditions, GP10 (0.78–100 μM) bound to HMGB1 full-length in a fast-on/fast-off and concentration-dependent manner with a K_D of 3.79×10^{-5} M (Fig. 4a&d & Table 1), indicating a transient interaction between GP10 and HMGB1. HMGB1 comprises three domains (A-box: 1–79 amino acids; B-box: 89–162 amino acids; acidic C-terminal: 186–215 amino acids), and key functions of HMGB1 are related to the A-box and B-box (Chen et al. 2022). As shown in Fig. 4b-c&e-f, 0.78 μM-100 μM GP10 interacts with both HMGB1 A-box and B-box in a concentration-dependent manner, with K_D of 9.86×10^{-5} and 5.08×10^{-5} M, respectively, suggesting GP10 is more likely to interact with HMGB1 B-box.

Table 1
The value of K_D for GP10 binding to HMGB1-full length, HMGB1 A-box HMGB1 B-box.

HMGB1-Full length	**K_D(M)**	**Rmax(RU)**	**offset(RU)**	**Chi^2(RU^2)**
	3.79×10^{-5}	**13.14**	**0.57**	**0.57**
HMGB1 A-box	9.86×10^{-5}	18.33	-0.54	0.11
HMGB1 B-box	5.08×10^{-5}	8.62	0.03	0.12

Table 1
The value of the binding constants (K_D) for GP10 binding to HMGB1-full length, HMGB1 A-box HMGB1 B-box.

HMGB1-Full length	**K_D(M)**	**Rmax(RU)**	**offset(RU)**	**Chi^2(RU^2)**
	3.79×10^{-5}	**13.14**	**0.57**	**0.57**
HMGB1 A-box	9.86×10^{-5}	18.33	-0.54	0.11
HMGB1 B-box	5.08×10^{-5}	8.62	0.03	0.12

Subsequently, UV absorption spectroscopy was employed to examine whether the interaction of GP10 to HMGB1 affects the conformation of HMGB1. As shown in Fig. 4g, with the increase in GP10 concentration (0-100μM), the shape of the absorption peaks changed: the strong absorption peak at 208 nm significantly weakened, while the shoulder peak at 273 nm gradually intensified with a slight red shift. This indicates altered polar microenvironments surrounding aromatic residues, as well as conformational changes in HMGB1.

When binding to ligands, structural conformation changes or alterations in the microenvironment surrounding the chromophoric amino acids of HMGB1 can exert a significant influence on the fluorescence spectrum of HMGB1 (Ye et al. 2023). As shown in Fig. 4h-i, with the increase in GP10 concentration (0-100 μM), a gradual quenching of the fluorescence emission peak of HMGB1 was observed, suggesting that the binding of GP10 to HMGB1 affects the conformational state of HMGB1. Meanwhile, a significant blue shift in the maximum emission wavelength was detected after the addition of GP10, indicating enhanced hydrophobicity in the vicinity of the chromophores of HMGB1 in the presence of GP10. The fitted Stern-Volmer curve shows an upward bending trend and gradually approaches the Y-axis, suggesting GP10 reduces the fluorescence intensity of HMGB1 via a combination of dynamic and static quenching. Collectively, these results indicate that the binding of GP10 to HMGB1 affects the structural conformation and microenvironment of HMGB1.

Furthermore, CD spectroscopy was used to investigate whether the binding of GP10 to HMGB1 affects the secondary structure of HMGB1. As shown in Fig. 4j, the CD spectra of HMGB1 in the absence and presence of GP10 were measured at 25 ℃. Consistent with previous reports, two negative bands appeared in the far-UV region at 208 nm (π-π* transition) and 222 nm (n-π* transition), corresponding to the α-helical structure of HMGB1 (Jiang et al. 2026). After the addition of GP10, no obvious change was observed in the characteristic peaks, but an increase in the intensity of the CD spectrum was detected. Meanwhile, the α-helix content of HMGB1 increased by 3.73% after the binding to GP10, while the percentage of random coils decreased, suggesting the conformational changes in the polypeptide backbone of HMGB1 (Table. 2).

Table 2
The relative contents of α-helix and random coil in HMGB1 in the absence or presence of GP10

HMGB1	**α-helix(%)**	**random coil (%)**
	41.79	**28.30**
HMGB1-GP10	45.52	26.69

We further investigated the particle size distribution and thermal stability using tryptophan fluorescence spectroscopy (Nano DSF). As shown in Fig. 4k and Table 3, the cumulant radius of HMGB1 at room temperature was 3.30 nm, whereas the addition of GP10 reduced this value to 2.86 nm. This result suggests that the binding of GP10 to HMGB1 leading to the folding or compaction of the protein molecule. As shown in Fig. 4l and Table. 4, the Tm value of HMGB1 was determined to be 48.83 ℃, whereas in the presence of GP10, the Tm value increased to 49.61 ℃, resulting in a ΔTm of 0.78 ℃. These findings further demonstrate that binding of GP10 to HMGB1 induces conformational changes that underlie the enhanced thermal stability of HMGB1.

Table 3
Particle size and distribution coefficient of HMGB1.

Samples	Cumulant Radius (nm)	PdI
HMGB1	3.30	0.07
HMGB1-GP10	2.86	0.06

Table 4
The Tm value (△Tm) of HMGB1 in the absence or presence of GP10.

Compounds	Tm(℃)	△Tm(℃)
HMGB1	48.83	-
HMGB1-GP10	49.61	0.78

Phe89 was identified as a critical residue for GP10-HMGB1 interaction

The above results indicate that the interaction between GP10 and HMGB1 can modulate the structure of HMGB1. Therefore, molecular docking was further employed to explore the interaction site of GP10 on HMGB1. As shown in Fig. 5a, GP10 associated with the HMGB1 B-box via hydrogen bonds formed with Lysine (Lys) 88 and Phe 89, with a binding energy (BN value) of -5.6, indicating effective binding with HMGB1 and consistent with the results of SPR. Previous studies have confirmed that HMGB1 can specifically bind to the TLR4-MD2 complex and RAGE receptor via the B-box domain, thereby mediating inflammation and inducing autophagy (He et al. 2018; Kim et al. 2025). The interaction between GP10 and the HMGB1 B-box is likely to further interfere with the protein-protein interaction of HMGB1 to receptors, consequently suppressing the downstream inflammation.

Based on molecular docking results, we successfully constructed and purified HMGB1-K88A and HMGB1-F89A mutants to further verify the binding site between GP10 and HMGB1 (Fig. 5b). The

results showed that HMGB1-K88A and HMGB1-F89A mutants still significantly induced the upregulation of *Il-1β*, *Il-6*, *Tnf-α*, and *Inos* mRNA expressions in BV2 cells ($p < 0.0001$, Fig. 5c-f). However, compared with wild-type HMGB1, the pro-inflammatory responses induced by the two mutants were significantly attenuated ($p < 0.05$). This result suggests that mutations at Lys88 and Phe89 may interfere with the binding of HMGB1 to TLR4/RAGE, thereby impairing its pro-inflammatory activity.

Furthermore, we compared the inhibitory effect of GP10 on the pro-inflammatory activities of wild-type HMGB1 and the two mutants. As shown in Fig. 5g-j, GP10 significantly inhibited wild-type HMGB1-induced inflammation in BV2 cells, while this inhibitory activity was notably abrogated after the mutation of Phe89, as evidenced by the failure of GP10 to effectively reduce the upregulation of *Il-1β*, *Il-6*, *Tnf-α*, and *Inos* mRNA expressions induced by HMGB1-F89A mutant. In contrast, GP10 still significantly

suppressed the upregulation of *Il-1β* ($p < 0.0001$), *Il-6* ($p < 0.0001$), *Tnf-α* ($p < 0.0001$), and *Inos* ($p < 0.05$) mRNAexpressions induced by HMGB1-K88A mutant. These results confirmed that Phe89 plays a crucial role in the specific binding between HMGB1 and GP10.

GP10 ameliorated pathological changes in the pilocarpine-induced mouse epilepsy model.

Given anti-inflammatory activity of GP10 *in vitro* of HMGB1 signaling, this study explored the potential therapeutic effects of GP10 in an epilepsy animal model. To simulate the effects of drug therapy on secondary seizures, a protocol was adopted where drugs were administered after initial model induction, followed by model re-induction after three days of drug treatment (Fig. 6a). Glycyrrhizin was previously demonstrated to ameliorate pilocarpine- and kainic acid-induced epilepsy models, serving as the positive control to evaluate GP10 efficacy (Li et al. 2019; Shang et al. 2025). After inducing the first pilocarpine-mediated epileptic seizure in all mice except those in the control group, the mice were grouped such that each group maintained a consistent Racine score level (Fig. 6b). Following 3 days of treatment according to the flowchart, 1 mg/kg, 3 mg/kg, and 10 mg/kg GP10 notably alleviated pilocarpine-induced secondary seizures ($p < 0.01$), while the 10 mg/kg GP10 group exhibited Racine scores comparable to those of the glycyrrhizin group (Fig. 6b).

Meanwhile, 3 h after the second modeling, serum HMGB1 concentration was markedly elevated in the epilepsy model group (Fig. 6c, $p < 0.001$), while 1 mg/kg, 3 mg/kg and 10 mg/kg GP10 substantially reduced serum HMGB1 concentration ($p < 0.05$). Notably, serum HMGB1 concentration in the 10 mg/kg GP10 group was lower than that in the 100 mg/kg glycyrrhizin group, suggesting GP10 reduced injury-induced passive HMGB1 release.

Hippocampal neuron loss is a key event driving post-seizure injuries (Liu et al. 2023). HE-stained sections quantified surviving neurons in the CA1, CA3, and CA4 regions. As shown in Fig. 6d-g, the model group exhibited obvious loss of hippocampal neurons in the CA1 ($p < 0.001$), CA3 ($p < 0.0001$) and CA4 regions ($p < 0.001$). 10 mg/kg GP10 substantially attenuated neuron loss in CA1 ($p < 0.001$), CA3 ($p < 0.001$), and CA4 ($p < 0.05$), with efficacy in CA1 and CA3 comparable to glycyrrhizin. Nissl staining of hippocampus (Fig. 6h-k) aligned with HE staining: the model group showed a significant reduction in Nissl bodies in CA1 ($p < 0.001$), CA3 ($p < 0.01$), and CA4 ($p < 0.001$), indicating neuronal loss, while 10 mg/kg GP10 notably increased Nissl body counts in CA1 ($p < 0.05$), CA3 ($p < 0.05$), and CA4 ($p < 0.001$), with ameliorative effects comparable to glycyrrhizin. In conclusion, GP10 mitigates hippocampal neuronal loss caused by epilepsy-induced abnormal excitability at a low dose, with efficacy similar to glycyrrhizin.

GP10 suppressed the neuroinflammation after pilocarpine-induced epilepsy in mice.

In animal models, GP10 notably improved behavioral performance and reduced neuronal injury in epileptic lesions. Given the demonstrated anti- inflammatory activity of GP10 on BV2 cells in vitro, we hypothesized that this effect might involve inhibition of post-epileptic inflammatory storm and mitigation of secondary seizures.

First, we detected mRNA expression of classic pro-inflammatory mediators (eg. *Il-1β*, *Il-6*, and *Tnf-α*) in hippocampal tissue. As shown in Fig. 7a-e, epilepsy model groups exhibited markedly elevated hippocampal mRNA levels of *Hmgb1* ($p < 0.01$), *Il-1β* ($p < 0.001$), *Il-6* ($p < 0.0001$), *Tnf-α* ($p < 0.0001$), and the oxidative stress marker *Ho-1* ($p < 0.001$). Treatment with different GP10 concentrations reversed upregulation of *Hmgb1* ($p < 0.05$), *Il-1β* ($p < 0.01$), *Il-6* ($p < 0.01$), and *Tnf-α* ($p < 0.01$) mRNA expression ($p < 0.05$), indicating GP10 inhibits pro-inflammatory factor transcription after epilepsy. GP10 at 3 and 10 mg/kg also considerably suppressed hippocampal *Ho-1* mRNA expression ($p < 0.05$), suggesting partial attenuation of oxidative stress post epilepsy (Fig. 7e). Notably, 10 mg/kg GP10 showed similar efficacy to glycyrrhizin in inhibiting *Hmgb1*, *Il-1β*, and *Ho-1* mRNA upregulation, demonstrating anti-inflammatory effects in epileptic animals at low doses.

Next, we investigated the effects of GP10 on HMGB1-associated inflammatory pathways and protein expression. As shown in Fig. 7f-l, epileptic models displayed markedly upregulated hippocampal expression level of NLRP3 ($p < 0.001$), p38 phosphorylation ($p < 0.001$), HMGB1 ($p < 0.0001$), NF-κB phosphorylation ($p < 0.0001$), HO-1 ($p < 0.0001$), and IL-1β ($p < 0.0001$). Administration of 10 mg/kg GP10 significantly normalized these protein levels ($p < 0.05$) and exhibited similar inhibitory effects to glycyrrhizin. These results confirm GP10 suppresses epilepsy- induced inflammatory cascade activation and downstream protein expression at low doses, thereby alleviating further lesion damage from post-epileptic inflammatory storm.

Discussion

Epilepsy is a common neurological disorder affecting all age groups, with major unmet clinical therapeutic demands. Accumulating studies highlight that HMGB1 signaling drives epileptic pathologies including neuronal hyperexcitability, BBB disruption, neuroinflammation. This study employed small molecules to demonstrate that targeted HMGB1 conformational modulation suppresses the pro-inflammatory effects, mitigating post-seizure secondary neuroinflammation-mediated brain injury and recurrent epilepsy progression. GP10 was characterized as a novel HMGB1 modulator and confirmed the anti-neuroinflammatory effects in preclinical epilepsy models. Overall, this work uncovers the vital role of HMGB1 conformational regulation in epilepsy treatment, laying theoretical and experimental groundwork for novel antiepileptic drug discovery.

Accumulated evidence links elevated HMGB1 in epileptic lesions and serum to seizure severity, making HMGB1 a promising seizure biomarker. Existing research has demonstrated that multiple substances including glycyrrhizin, inflachromene, microRNA, and *Gardenia jasminoides* extracts can alleviate seizure symptoms in various animal models by suppressing the abnormal upregulation and translocation of HMGB1 (Dai et al. 2023; Fu et al. 2020; Sun et al. 2025; Wei, Ou, Meng, Sun, Zhang, Lu and Wu 2025). Notably, as a DAMP, HMGB1 binds TLR4/RAGE to initiate glia-mediated neuroinflammation. This mechanism acts as a critical pathway that persistently triggers chronic central inflammation during the interictal period of epilepsy, thereby lowering the seizure threshold, and ultimately leading to recurrent epileptic seizures. On this basis, this study hypothesizes that targeted

intervention against accumulated HMGB1 in epileptic lesions may effectively delay and inhibit the recurrent progression of epilepsy (Fig. 8).

The structural diversity of natural products offers great potential for drug discovery. To test the hypothesis that targeted HMGB1 modulation alleviates epileptic seizures by suppressing the pro-inflammatory activity of HMGB1, this study employed naturally derived THPBs as molecular probes. These compounds exhibit favorable BBB permeability, supporting their utility in anti-epileptic drug development (Nesbit and Phillips 2020). Although several naturally derived HMGB1 inhibitors (e.g., glycyrrhizic acid, celastrol, and curcumin) have been identified, selective HMGB1 inhibitors remain scarce. Accordingly, following primary screening for HMGB1 inhibitory activity, candidates were further evaluated in LPS-induced inflammation models to exclude direct TLR4/RAGE antagonism and confirm HMGB1 selectivity. Results showed that the candidate compound GP10 rapidly suppressed TLR4/RAGE-triggered NF-κB and MAPK signaling activation, and reduced aberrant exprssion of pro-inflammatory factors. Upon prolonged drug treatment, GP10 inhibited NO release from activated BV2 cells. Although efficacy varied across inflammatory markers at both mRNA and protein levels, GP10 comprehensively suppressed HMGB1-TLR4/RAGE-driven inflammatory cascade. Compared with classic HMGB1 inhibitor glycyrrhizin, GP10 effectively inhibited the pro-inflammatory activity of HMGB1 at lower concentrations with enhanced selectivity.

Prior work has demonstrated that the binding of small molecules to HMGB1 usually triggers HMGB1 conformational changes (Knapp et al. 2004). We therefore hypothesized that the activity and selectivity of GP10 against HMGB1 in the cell model involve direct interaction and conformational modulation. Our study confirmed that GP10 interacts with HMGB1 in fast on/off kinetics (Kd ≈ 37.9 μM), exhibiting stronger affinity than glycyrrhizin (~ 150 μM) (Sgrignani et al. 2021). GP10 also showed lower K_D for B-box than A-box, suggesting B-box preference. Combined UV, fluorescence, and CD spectra revealed that the binding of GP10 significantly alters the spatial conformation of HMGB1 and increases the hydrophobicity of the microenvironment surrounding chromogenic amino acid residues. The binding of GP10 to HMGB1 also induced protein structural compaction and enhanced the thermal stability of HMGB1. Overall, the interaction of GP10 to HMGB1 induced conformational rearrangements of HMGB1, corresponding to the selective suppression of GP10 on HMGB1-mediated inflammation *in vitro*.

To elucidate the molecular mechanism underlying GP10-induced conformational regulation of HMGB1, molecular docking was employed to predict the binding sites. The docking results revealed that GP10 interacts with the B-box via hydrogen bonds at Lys88 and Phe89, representing the most stable conformation. This was corroborated by SPR data showing a lower K_D for B-box than for A-box. Our observations differ from a previous report that berberine targets the A-box, possibly due to differing substituents on the A and D rings (Jiang et al. 2026; Shi et al. 2021). Functional validation with point mutants confirmed Phe89 as the critical residue, since alanine substitution of Phe89 abolished the inhibition of GP10 on mutant HMGB1-induced inflammation. Notably, the HMGB1-F89A mutant elicited weaker inflammatory activity compared to wild-type HMGB1. This is likely because the critical motif mediating HMGB1- TLR4 interaction residing within the Phe89-Glutamic acid (Glu)108 of the B-box (Li et

al. 2003). Collectively, this study identifies the pivotal binding residue for GP10-HMGB1 interaction and further supports the selective mechanism by which GP10 attenuates HMGB1 pro-inflammatory activity through direct binding.

Accumulating evidence indicates HMGB1-mediated neuroinflammation impairs the BBB, lowers seizure threshold, and accelerates epilepsy progression (Arias-Carrión et al. 2026; Shokr and Eladawy 2025). In this study, GP10 markedly alleviated recurrent seizures, presumably by specifically binding lesion-released HMGB1 and abrogating HMGB1-triggered secondary lesion injury. Serum HMGB1 levels were reduced after GP10 treatment, implying suppression of HMGB1 intracellular translocation and extracellular secretion. Epilepsy-induced hyperactive neuronal firing triggers neuronal apoptosis and hippocampal dysfunction (Li et al. 2024; Zhou et al. 2026). GP10 treatment elevated neuronal survival in all hippocampal subregions. Mechanistically, GP10 attenuated seizure-stimulated overexpression of IL-1β, IL-6, TNF-α and hyperactivation of NF-κB/MAPK cascades. These *in vivo* results validate our *in vitro* observation that GP10 suppresses HMGB1-dependent neuroinflammation. Epileptic pathology correlates closely with oxidative stress imbalance. Disrupted redox homeostasis accumulates reactive oxygen/nitrogen species, causing oxidative biomolecular damage and cell death (Ji et al. 2025). GP10 downregulated elevated HO-1 mRNA and protein in model mice, relieving neuronal oxidative injury to preserve neuron viability. Notably, GP10 achieved equivalent therapeutic effects at lower doses than glycyrrhizin, supporting its favorable druggable potential.

The present study has several limitations. While the F89A mutation evidently alleviated HMGB1-mediated inflammation, direct evidence demonstrating how this residue regulates the binding mode of HMGB1 with PRRs is still lacking. We validated the anti-epileptic efficacy of GP10 in a pilocarpine-induced mouse epilepsy model. Additional validation experiments in kainic acid- or pentylenetetrazol-induced epileptic models are required to confirm the generalized anti-seizure activity of GP10. Moreover, further intervention experiments using HMGB1 neutralizing antibodies should be performed to consolidate the *in vivo* mechanism by which GP10 targets HMGB1. Finally, from a druggability standpoint, systematic pharmacokinetic studies are necessary to characterize the *in vivo* absorption, distribution and metabolism profiles of GP10, providing experimental support for the subsequent clinical translation.

Conclusion

Collectively, the present study centers on a core research logic: small molecules bind HMGB1 to alter its spatial conformation, block HMGB1-mediated neuroinflammation triggered by HMGB1 acting as a DAMP, and ultimately alleviate recurrent epileptic seizures. Meanwhile, we identified GP10 as a novel HMGB1 modulator. *In vitro* functional assays validated that GP10 exerts selective inhibitory effects against HMGB1-initiated inflammatory cascades. Further molecular characterization demonstrated that GP10 interacts with the B-box domain of HMGB1 via the Phe89 residue, and this intermolecular binding drives substantial conformational change in HMGB1. In pilocarpine-induced epileptic murine models, GP10 administration significantly alleviated recurrent seizures, attenuated neuronal loss, and suppressed

lesion-associated oxidative stress and inflammatory infiltration. Follow-up investigations will further dissect the target-specific mechanism of GP10 *in vivo* and characterize the bioavailability for clinical translation valuation. This research framework may promote novel antiepileptic drug development and provide original experimental support for therapeutic discovery.

Abbreviations

AEDs
Antiepileptic drugs
BBB
blood-brain barrier
BSA
bovine serum albumin
CD
circular dichroism
CNS
central nervous system
DAMP
damage-associated molecular pattern
DMEM
Dulbecco's modified eagle medium
DMSO
dimethyl sulfoxide
ELISA
enzyme-linked immunosorbnent assay
ERK
extracellular regulated protein kinases
FBS
fetal bovine serum
GAPDH
glyceraldehyde – 3-phosphate dehydrogenase
Glu
Glutamic acid
HE
hematoxylin-eosin
HO-1
heme oxygenase 1
Inos
inducible nitric oxide synthase
IL

interleukin
IPTG
isopropyl-β-D-thiogalactopyranoside
LB
Luria-Bertani
LPS
lipopolysaccharide
Lys
lysine
MAPK
mitogen-activated protein kinase
MTT
Methyl thiazolyl tetrazolium
NF-κB
nuclear factor-κB
NLRP3
NOD-like receptor thermal protein domain-associated protein 3
NO
nitric oxide
OD
optical density
PBS
phosphate buffered saline
Phe
phenylalanine
PRRs
pattern recognition receptors
P/S
penicillin-streptomycin
qRT-PCR
quantitative reverse transcription polymerase chain reaction
RAGE
receptor for advanced glycation end products
RU
response unit
SAR
structure-activity relationship
SEM
standard error of the mean
SPR

surface plasmon resonance
TBS
tris buffered saline
THPBs
tetrahydroprotoberberine derivatives
TLR4
toll-like receptor 4
Tm
melting temperature
TNF
tumor necrosis factor.

Declarations

Authors information

Corresponding Authors

*__Corresponding author: Jian Zhang__– *Department of Traditional Chinese Medicine Resources, China Pharmaceutical University, Nanjing 211198, China; Xizang University of Tibetan Medicine, Lhasa, 850000, China,* Email:*1020071849@cpu.edu.cn.*

**__Co-corresponding author: Haixia Ge__– *School of Life Sciences, Huzhou Normal University, Huzhou 313000, China;* Email: *ghxzwx2012@163.com.*

Authors

Liaoxi Tan – *Department of Traditional Chinese Medicine Resources, China Pharmaceutical University, Nanjing 211198, China; Email: 3023024178@stu.cpu.edu.cn.*

Xuewa Jiang – *Department of Traditional Chinese Medicine Resources, China Pharmaceutical University, Nanjing 211198, China; Email: 3123034198@stu.cpu.edu.cn.*

Junyi Ye – *Department of Traditional Chinese Medicine Resources, China Pharmaceutical University, Nanjing 211198, China; Email: 3222020700@stu.cpu.edu.cn.*

Weihang Yao – *Department of Traditional Chinese Medicine Resources, China Pharmaceutical University, Nanjing 211198, China; Email: 3223020766@stu.cpu.edu.cn.*

Pingping Shen – *School of Chemical Engineering, Xuzhou College of Industrial Technology, Xuzhou 221140, China;* Email: *shpp1127@163.com.*

Author Contributions

Conceptualization: Jian Zhang; Methodology: Liaoxi Tan, Xuewa Jiang; Formal analysis and investigation: Liaoxi Tan, Xuewa Jiang, Junyi Ye, Weihang Yao, Pingping Shen; Writing - original draft preparation: Liaoxi Tan; Writing - review and editing: Jian Zhang, Liaoxi Tan, Xuewa Jiang; Funding acquisition: Jian Zhang; Resources: Jian Zhang,Haixia Ge; Supervision: Jian Zhang.

Declarations

Competing interest The authors declare that they have no known competing financial interests or personal relationships that could have appeared to influence the work reported in this paper.

Ethics Approval All animal experiments were conducted in accordance with the Guide for the Care and Use of Laboratory Animals of the National Institutes of Health (NIH publication No. 8023, revised 1978) and approved by the Laboratory Animal Management Committee of China Pharmaceutical University (YSL-202601033).

Funding This study was supported by the financial support from Central Funds Guiding the Local Science and Technology Development, Science and Technology Department of Inner Mongolia (2025ZY0127).The authors would like to thank China Pharmaceutical University and the Department of Traditional Chinese Medicine Resources for for the support.

References

1. Arias-Carrión O, de Ita Rodríguez, Yu J P (2026) Innate immune signalling, neuroinflammation and network plasticity in temporal lobe epilepsy. Front Pharmacol 17. https://doi.org/10.3389/fphar.2026.1770964
2. Ava H, R. L.J (2024) Role of inflammasomes and neuroinflammation in epilepsy. Immunol Rev 329. https://doi.org/10.1111/imr.13421
3. Balaha MF, Alamer AA, Abdel-Kader MS, Alharthy KM (2023) Ameliorative Potential of (-) Pseudosemiglabrin in Mice with Pilocarpine-Induced Epilepsy: Antioxidant, Anti-Inflammatory, Anti-Apoptotic, and Neurotransmission Modulation. Int J Mol Sci 24. https://doi.org/10.3390/ijms241310773
4. Brennan GP, Garcia-Curran MM, Patterson KP, Luo R, Baram TZ (2021) Multiple Disruptions of Glial-Neuronal Networks in Epileptogenesis That Follows Prolonged Febrile Seizures. Front Neurol 12. https://doi.org/10.3389/fneur.2021.615802
5. Bu J, Zhang X, Li Q, Ma Y, Hu Z, Yang J, Liu X, Wang R, Jiao X, Chen T et al (2022) Catalytic promiscuity of O-methyltransferases from Corydalis yanhusuo leading to the structural diversity of benzylisoquinoline alkaloids. Hortic Res. https://doi.org/10.1093/hr/uhac152
6. Chen R, Kang R, Tang D (2022) The mechanism of HMGB1 secretion and release. Exp Mol Med 54:91–102. https://doi.org/10.1038/s12276-022-00736-w
7. Dai S-j, Shao Y-y, Zheng Y, Sun J-y, Li Z-s, Shi J-y, Yan M-q, Qiu X-y, Xu C-l., Cho W-s et al (eds) (2023) Inflachromene attenuates seizure severity in mouse epilepsy models via inhibiting HMGB1

translocation. Acta Pharmacol. Sin. 44: 1737-47. https://doi.org/10.1038/s41401-023-01087-6

8. Eberhard J, Henning L, Fülle L, Knöpper K, Böhringer J, Graelmann FJ, Hänschke L, Kenzler J, Brosseron F, Heneka MT et al (2024) Ablation of CCL17-positive hippocampal neurons induces inflammation-dependent epilepsy. Epilepsia 66:554–568. https://doi.org/10.1111/epi.18200
9. Feng Z, Meng F, Huo F, Zhu Y, Qin Y, Gui Y, Zhang H, Lin P, He Q, Li Y et al (2024) Inhibition of ferroptosis rescues M2 macrophages and alleviates arthritis by suppressing the HMGB1/TLR4/STAT3 axis in M1 macrophages. Redox Biol 75. https://doi.org/10.1016/j.redox.2024.103255
10. Fu M, Tao J, Wang D, Zhang Z, Wang X, Ji Y, Li Z (2020) Downregulation of MicroRNA-34c-5p facilitated neuroinflammation in drug-resistant epilepsy. Brain Res 1749. https://doi.org/10.1016/j.brainres.2020.147130
11. Ge H, Zhang W, Yuan K, Xue H, Cheng H, Chen W, Xie Y, Zhang J, Xu X, Yang P (2021) Design, synthesis, and biological evaluation of novel tetrahydroprotoberberine derivatives to reduce SREBPs expression for the treatment of hyperlipidemia. Eur J Med Chem 221. https://doi.org/10.1016/j.ejmech.2021.113522
12. Grote A, Heiland D-H, Taube J, Helmstaedter C, Ravi VM, Will P, Hattingen E, Schüre J-R, Witt J-A, Reimers A et al (2023) Hippocampal innate inflammatory gliosis only' in pharmacoresistant temporal lobe epilepsy. Brain 146:549–560. https://doi.org/10.1093/brain/awac293
13. Guo A, Zhang H, Li H, Chiu A, García-Rodríguez C, Lagos CF, Sáez JC, Lau CG (2022) Inhibition of connexin hemichannels alleviates neuroinflammation and hyperexcitability in temporal lobe epilepsy. Proc Natl Acad Sci U S A 119:e2213162119. https://doi.org/10.1073/pnas.2213162119
14. He M, Bianchi ME, Coleman TR, Tracey KJ, Al-Abed Y (2018) Exploring the biological functional mechanism of the HMGB1/TLR4/MD-2 complex by surface plasmon resonance. Mol Med 24. https://doi.org/10.1186/s10020-018-0023-8
15. Jehi L (2025) Advances in Therapy for Refractory Epilepsy. Annu Rev Med 76:389–402. https://doi.org/10.1146/annurev-med-050522-034458
16. Ji D, Mylvaganam S, Ravi Chander P, Tarnopolsky M, Murphy K, Carlen P (2025) Mitochondria and oxidative stress in epilepsy: advances in antioxidant therapy. Front Pharmacol 15. https://doi.org/10.3389/fphar.2024.1505867
17. Jiang X, Yi S, Shen P, Raj R, Zhang J, Ge H (2026) Insights on the synergistic effects of glycyrrhetinic acid and isoliquiritigenin on HMGB1-induced inflammation by multi-spectroscopic and molecular docking studies. Spectrochim Acta Part A 344. https://doi.org/10.1016/j.saa.2025.126726
18. Jiang X, Yi S, Shen P, Raj R, Zhang J, Ge H (2026) Insights on the synergistic effects of glycyrrhetinic acid and isoliquiritigenin on HMGB1-induced inflammation by multi-spectroscopic and molecular docking studies. Spectrochim Acta Part A 344:126726. https://doi.org/https://doi.org/10.1016/j.saa.2025.126726
19. Kim HJ, Han CW, Jeong MS, Kwon T-J, Choi JY, Jang SB (2025) Cryo-EM structure of HMGB1-RAGE complex and its inhibitory effect on lung cancer. Biomed Pharmacother 187:118088.

https://doi.org/https://doi.org/10.1016/j.biopha.2025.118088

20. Knapp S, Müller S, Digilio G, Bonaldi T, Bianchi M, Musco G (2004) The long acidic tail of high mobility group box 1 (HMGB1) protein forms an extended and flexible structure that interacts with specific residues within and between the HMG boxes. Biochemistry 43:11992–11997. https://doi.org/10.1021/bi049364k
21. Krishnamurthy. BK (2025) Epilepsy. ANN INTERN MED 178: ITC49-ITC64. https://doi.org/10.7326/annals-25-00494
22. Li C, Cai Y, Chen Y, Tong J, Li Y, Liu D, Wang Y, Li Z, Wang Y, Li Q (2024) ABCG2 shields against epilepsy, relieves oxidative stress and apoptosis via inhibiting the ISGylation of STAT1 and mTOR. Redox Biol 75. https://doi.org/10.1016/j.redox.2024.103262
23. Li J, Kokkola R, Tabibzadeh S, Yang R, Ochani M, Qiang X, Harris HE, Czura CJ, Wang H, Ulloa L et al (2003) Structural basis for the proinflammatory cytokine activity of high mobility group box 1. Mol Med 9:37–45
24. Li Y-j, Wang L, Zhang B, Gao F, Yang C-M (2019) Glycyrrhizin, an HMGB1 inhibitor, exhibits neuroprotective effects in rats after lithium-pilocarpine-induced status epilepticus. J Pharm Pharmacol 71:390–399. https://doi.org/10.1111/jphp.13040
25. Lim G, Kim HR, Yoo C, Oh YK, Park YS, Park S, Jang S, Priscilla L, Lee DY (2025) Mucoadhesive and Self-Assembled Chitosan Oligosaccharide-Glycyrrhizin Nanoparticle for Oral Nanotherapeutic in Inflammatory Bowel Disease. ACS Nano 19:31169–31182. https://doi.org/10.1021/acsnano.5c09985
26. Liu C, Zhao X-M, Wang Q, Du T-T, Zhang M-X, Wang H-Z, Li R-P, Liang K, Gao Y, Zhou S-Y et al (2023) Astrocyte-derived SerpinA3N promotes neuroinflammation and epileptic seizures by activating the NF-κB signaling pathway in mice with temporal lobe epilepsy. J Neuroinflammation 20. https://doi.org/10.1186/s12974-023-02840-8
27. Luo R, Yao Y, Chen Z, Sun X (2025) An examination of the LPS-TLR4 immune response through the analysis of molecular structures and protein–protein interactions. Cell Commun Signal 23. https://doi.org/10.1186/s12964-025-02149-4
28. Ma L, Xu M, Xu S, Guo X, Zong W, Zhao X, Yang Z, Liu G, Shen L (2025) HMGB1 downregulates DDX3 to activate the MAPK pathway, promoting the progression of colorectal cancer. Cancer Gene Ther 32:1307–1318. https://doi.org/10.1038/s41417-025-00963-z
29. Meng Y, Jiang X, Raj R, Shen P, Zhang J (2025) Exploring the molecular interaction of celastrol and HMGB1 by multi-spectra analysis. J Biomol Struct Dyn 1–15. https://doi.org/10.1080/07391102.2025.2530041
30. Nesbit MO, Ahn S, Zou H, Floresco SB, Phillips AG (2024) Potentiation of prefrontal cortex dopamine function by the novel cognitive enhancer d-govadine. Neuropharmacology 246:109849. https://doi.org/https://doi.org/10.1016/j.neuropharm.2024.109849
31. Nesbit MO, Phillips AG (2020) Tetrahydroprotoberberines: A Novel Source of Pharmacotherapies for Substance Use Disorders? Trends Pharmacol Sci 41:147–161.

https://doi.org/10.1016/j.tips.2019.12.007

32. Özbay Kurt FG, Cicortas B-A, Balzasch BM, De la Torre C, Ast V, Tavukcuoglu E, Ak C, Wohlfeil SA, Cerwenka A, Utikal J et al (2024) S100A9 and HMGB1 orchestrate MDSC-mediated immunosuppression in melanoma through TLR4 signaling. J ImmunoTher Cancer 12. https://doi.org/10.1136/jitc-2024-009552
33. Park J-H, Seo YH, Jang J-H, Jeong C-H, Lee S, Park B (2017) Asiatic acid attenuates methamphetamine-induced neuroinflammation and neurotoxicity through blocking of NF-kB/STAT3/ERK and mitochondria-mediated apoptosis pathway. J Neuroinflammation 14. https://doi.org/10.1186/s12974-017-1009-0
34. Ravizza T, Scheper M, Di Sapia R, Gorter J, Aronica E, Vezzani A (2024) mTOR and neuroinflammation in epilepsy: implications for disease progression and treatment. Nat Rev Neurosci 25:334–350. https://doi.org/10.1038/s41583-024-00805-1
35. Ravizza T, Terrone G, Salamone A, Frigerio F, Balosso S, Antoine DJ, Vezzani A (2018) Brain Behav Immun 72:14–21. https://doi.org/10.1016/j.bbi.2017.10.008. High Mobility Group Box 1 is a novel pathogenic factor and a mechanistic biomarker for epilepsy
36. Sgrignani J, Cecchinato V, Fassi EMA, D'Agostino G, Garofalo M, Danelon G, Pedotti M, Simonelli L, Varani L, Grazioso G et al (2021) Systematic Development of Peptide Inhibitors Targeting the CXCL12/HMGB1 Interaction. J Med Chem 64:13439–13450. https://doi.org/10.1021/acs.jmedchem.1c00852
37. Shang L, Guo H, Gong D (2025) Molecular Mechanism of Compound Glycyrrhizin in Kainic Acid-Induced Epilepsy in Rat Model. Mol Biotechnol. https://doi.org/10.1007/s12033-025-01460-2
38. Shi J, Xu H, Cavagnaro MJ, Li X, Fang J (2021) Blocking HMGB1/RAGE Signaling by Berberine Alleviates A1 Astrocyte and Attenuates Sepsis-Associated Encephalopathy. Front Pharmacol 12. https://doi.org/10.3389/fphar.2021.760186
39. Shi Y, Zhang L, Teng J, Miao W (2018) HMGB1 mediates microglia activation via the TLR4/NF-κB pathway in coriaria lactone induced epilepsy. Mol Med Rep. https://doi.org/10.3892/mmr.2018.8485
40. Shokr MM, Eladawy RM (2025) HMGB1: Different secretion pathways with pivotal role in epilepsy and major depressive disorder. Neuroscience 570:55–67. https://doi.org/10.1016/j.neuroscience.2025.02.023
41. Sun M, Yuan Z, Li M, Ji X, Huang L, Yang Y, Qiu X, Zhang S, Jiang X, Lv Q et al (2025) Gardeniae Fructus extract terminates refractory status epilepticus with a wide time window through inhibiting neuroinflammation. Phytomedicine 142. https://doi.org/10.1016/j.phymed.2025.156770
42. Wang X, Liu Y, Li M, Ju Y, Tang J, Chen T, Lin X, Gu N, Yang F (2023) Neuroinflammation catching nanobubbles for microglia-neuron unit modulation against epilepsy. Biomaterials 302. https://doi.org/10.1016/j.biomaterials.2023.122302
43. Wei L, Ou S, Meng Y, Sun L, Zhang L, Lu Y, Wu Y (2025) Glycyrrhizin as a potential disease-modifying therapy for epilepsy: insights into targeting pyroptosis to exert neuroprotective and anticonvulsant effects. Front Pharmacol 15. https://doi.org/10.3389/fphar.2024.1530735

44. Xie Y, Yu N, Chen Y, Zhang K, Ma H-Y, Di Q (2017) HMGB1 regulates P-glycoprotein expression in status epilepticus rat brains via the RAGE/NF-κB signaling pathway. Mol Med Rep 16:1691–1700. https://doi.org/10.3892/mmr.2017.6772
45. Ye J, Huang Y, Jiang X, Shen P, Zhang C, Zhang J (2023) Research on the interaction of astragaloside IV and calycosin in Astragalus membranaceus with HMGB1. Chin. Med 18. https://doi.org/10.1186/s13020-023-00789-7
46. Ye J, Huang Y, Jiang X, Shen P, Zhang C, Zhang J (2023) Research on the interaction of astragaloside IV and calycosin in Astragalus membranaceus with HMGB1. Chin Med 18:81. https://doi.org/10.1186/s13020-023-00789-7
47. Zheng X, Zheng W, Zhou J, Gao X, Liu Z, Han N, Yin J (2018) Study on the discrimination between Corydalis Rhizoma and its adulterants based on HPLC-DAD-Q-TOF-MS associated with chemometric analysis. J Chromatogr B Analyt Technol Biomed Life Sci 1090:110–121. https://doi.org/10.1016/j.jchromb.2017.10.028
48. Zhou Z, Zhang P, Jiang Y, Xu Y, Liu F, Chen X, Chen D, Tang W, Liao R, Liu L (2026) Astrocytic LCN2 drives neuronal dysfunction in epilepsy by suppressing tunnel nanotube-mediated mitochondrial transfer via NLRP3 inflammasome activation. Free Radical Biol Med 244:84–106. https://doi.org/10.1016/j.freeradbiomed.2025.11.061
49. Zurolo E, Iyer A, Maroso M, Carbonell C, Anink JJ, Ravizza T, Fluiter K, Spliet WG, van Rijen PC, Vezzani A et al (2011) Activation of Toll-like receptor, RAGE and HMGB1 signalling in malformations of cortical development. Brain 134:1015–1032. https://doi.org/10.1093/brain/awr032

Figures

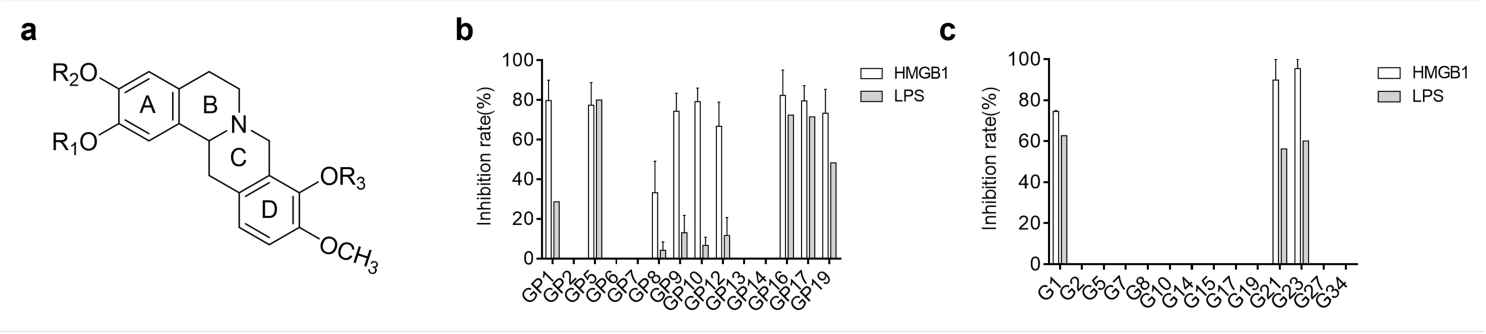


Figure 1

Screening THPBs that selectively suppress HMGB1 pro-inflammatory activity. (**a**) The skeleton of THPBs. (**b**) Inhibition rate of GPs on TNF-α release from BV2 cells induced by 5 μg/mL HMGB1 or 1 μg/mL LPS for 12 h. (**c**) Inhibition rate of Gs on TNF-α release from BV2 cells induced by 5 μg/mL HMGB1 or 1 μg/mL LPS for 12 h. All bar graphs represent mean ± SEM, n=3.

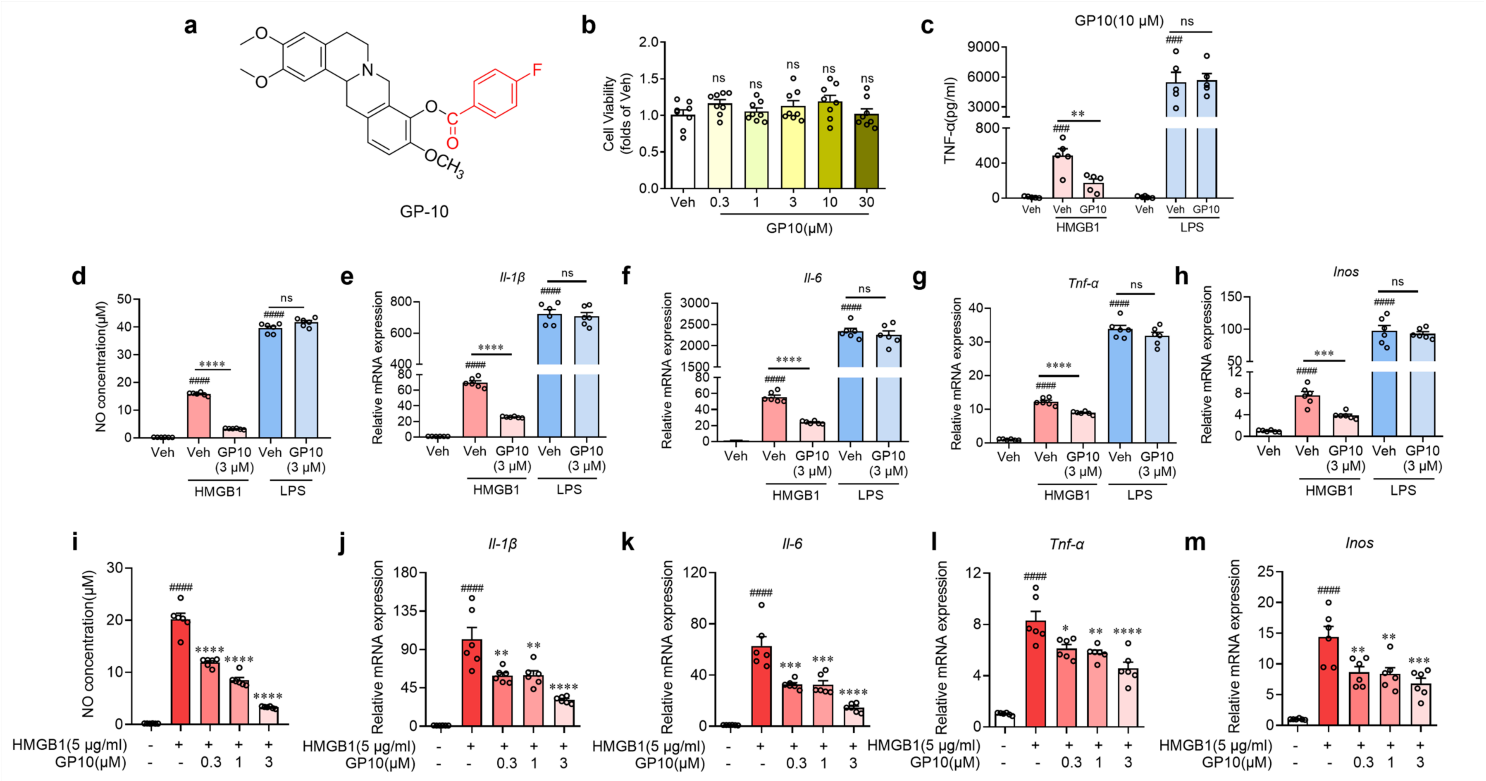


Figure 2

GP10 alleviated HMGB1-induced inflammatory factors expression in BV2 cells. (**a**) Structure of GP10. (**b**) MTT cell viability analysis of BV2 cells. (**c**) Quantification of TNF-α release from BV2 cell. (**d**) Quantification of NO production from BV2 cells. (**e**-**h**) Relative mRNA expression of *Il-1β*, *Il-6*, *Tnf-α*, and *Inos*. (**i**) Quantification of NO production from BV2 cells. (**j**-**m**) Relative mRNA expression of *Il-1β*, *Il-6*, *Tnf-α*, and *Inos*. Data are represented as mean ± SEM (n ≥ 5). Statistical analysis was performed using unpaired Student's t-test or one-way ANOVA, ### $p < 0.001$, #### $p < 0.0001$ versus Veh; * $p < 0.05$, ** $p < 0.01$, *** $p < 0.001$, **** $p < 0.0001$ versus HMGB1; ns, no significance versus LPS.

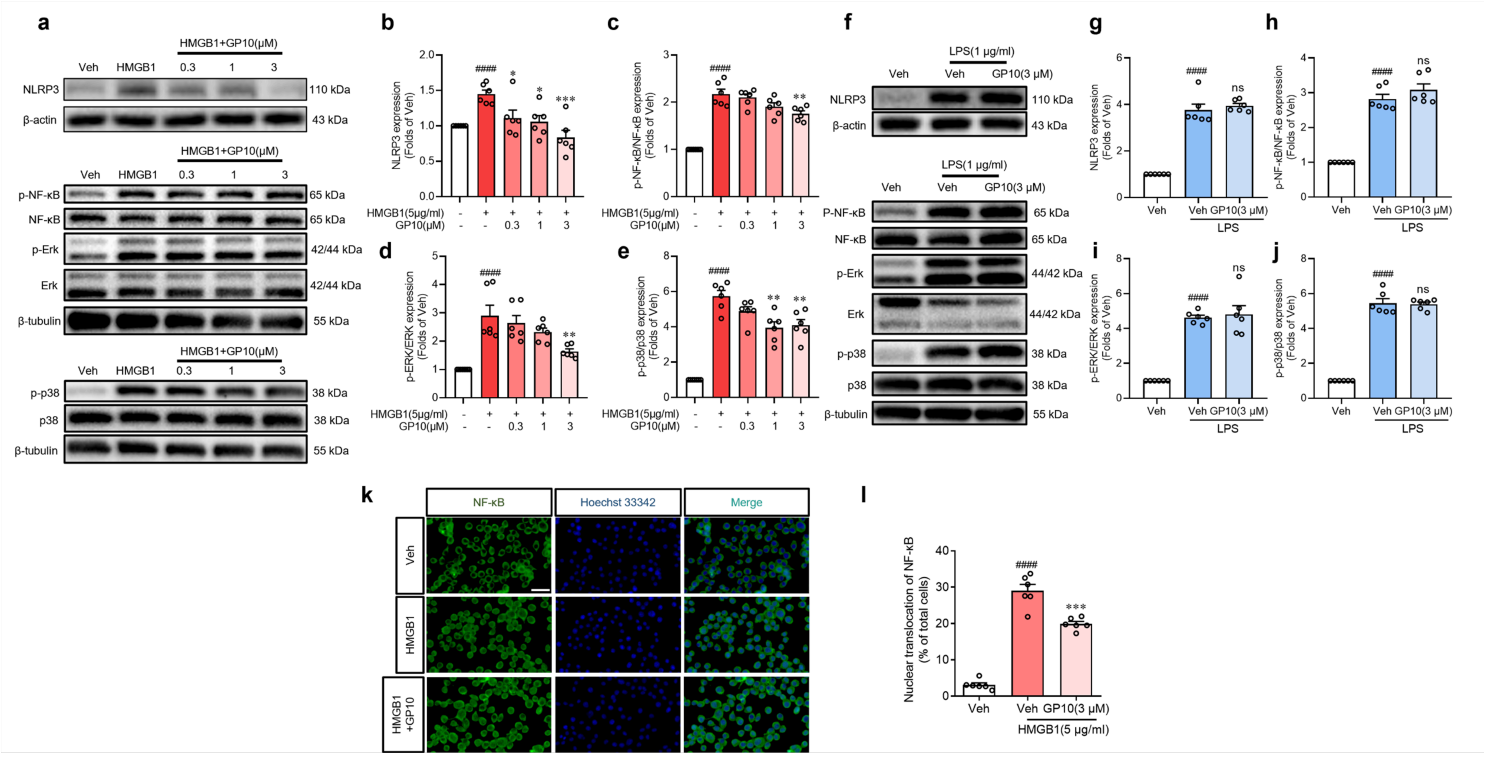


Figure 3

GP10 inhibited HMGB1-induced activation of inflammatory pathways in BV2 cells. (**a**-**j**) Western blot analysis of NLRP3, NF-κB phosphorylation, p38 MAPK phosphorylation, and ERK phosphorylation. (**k**-**l**) NF-κB traslocation detected by Immunofluorescence. Scale bar, 25 μm. Data are represented as mean ± SEM (n > 5). Statistical analysis was performed using unpaired Student's t-test or one-way ANOVA, #### $p < 0.0001$ versus Veh; * $p < 0.05$, ** $p < 0.01$, *** $p < 0.001$ versus HMGB1; ns, no significance versus LPS.

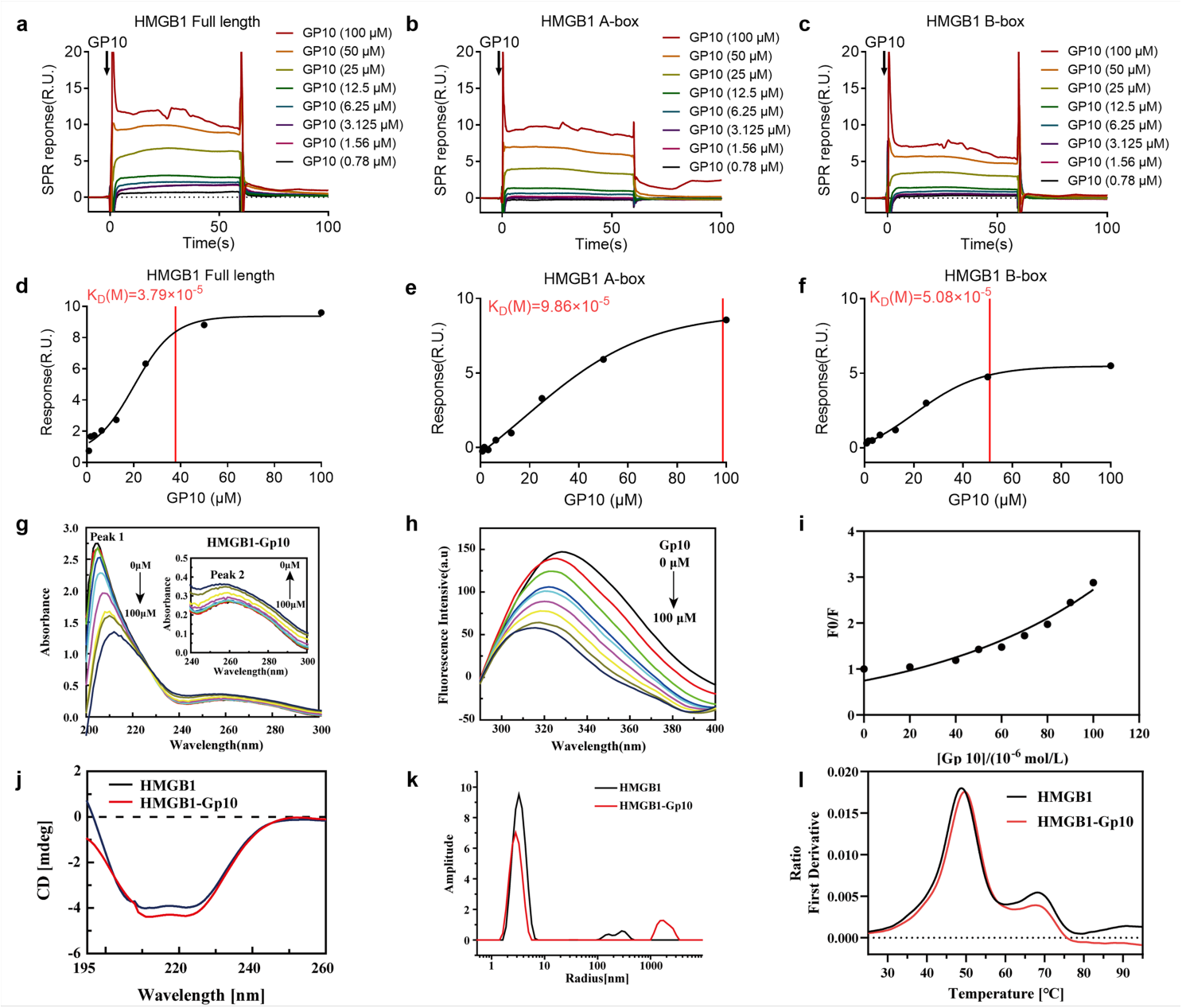


Figure 4

GP10 bound HMGB1 to alter its spatial conformation. (**a**-**f**) SPR assay and qualification of molecule-protein interaction. (**g**) UV absorption spectra (λ = 200-300 nm) of HMGB1 (3 μM) without or with different concentrations of GP10 (5, 10, 20, 40, 60, 80, 100 μM). (**h**-**i**) Steady state fluorescence spectra and Stern-Volmer plot for fluorescence quenching of HMGB1 on GP10addition. (**j**) The CD spectrum of HMGB1 binding to GP10. (**k**) The particle size of HMGB1 in the absence and presence of GP10. (**l**) First derivative diagram of the melting curve of HMGB1 in the absence and presence of GP10.

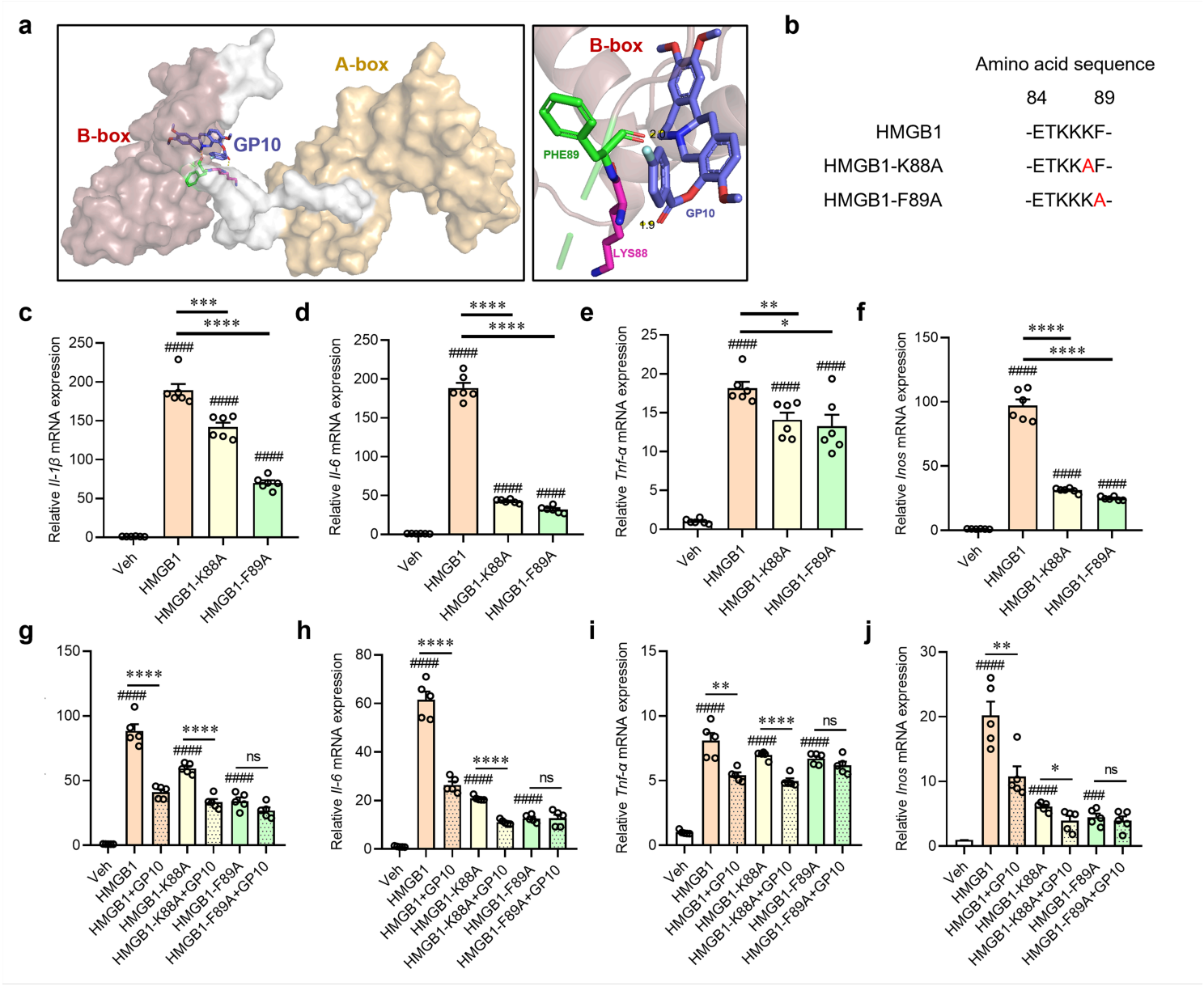


Figure 5

Phe89 is critical for the interaction between GP10 and HMGB1. (**a**) The molecular docking analysis of interaction between HMGB1 and GP10. (**b**) The amino acid sequences of wild-type HMGB1, HMGB1-K88A, and HMGB1-F89A. (**c**-**j**) Relative mRNA expression of *Il-1β*, *Il-6*, *Tnf-α*, and *Inos*. Data are represented as mean ± SEM(n ≥ 5). Statistical analysis was performed using unpaired Student's t-test; ### $p < 0.001$, #### $p < 0.0001$ versus Veh; * $p < 0.05$, ** $p < 0.01$, *** $p < 0.001$, **** $p < 0.0001$ versus HMGB1/HMGB1-K88A; ns, no significance versus HMGB1-F89A.

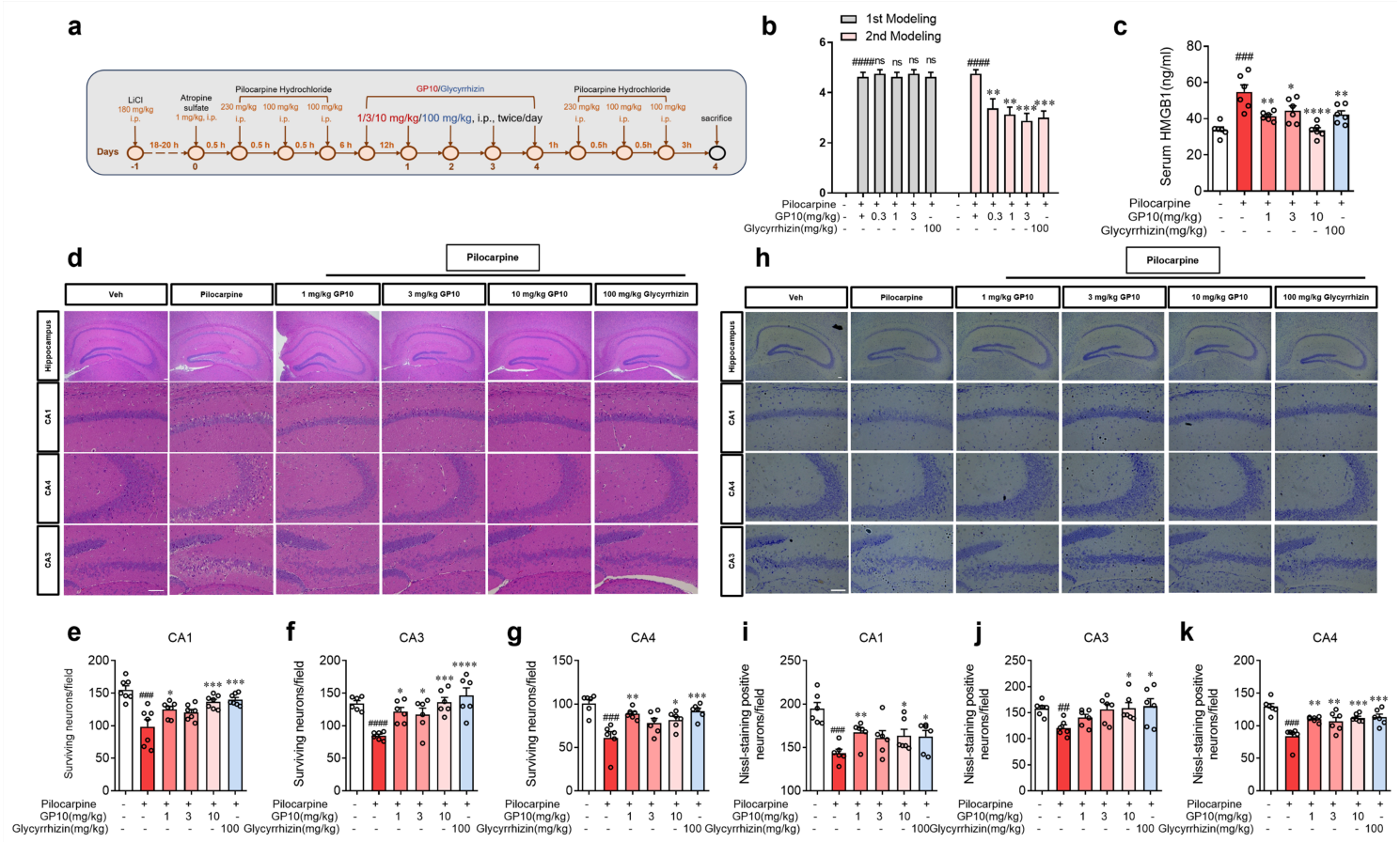


Figure 6

GP10 improved the neuronal loss in the lesion area of pilocarpine-induced epilepsy mouse models. (**a**) Schematic illustration depicting the establishment of the pilocarpine-induced epilepsy mouse model and the administration of GP10 (1, 3, and 10 mg/kg) or glycyrrhizin (100 mg/kg). (**b**-**c**) Quantification of Racine scores and Serum HMGB1 concentrations of mice treated with Veh, pilocarpine, pilocarpine+1 mg/kg GP10, pilocarpine+3 mg/kg GP10, pilocarpine+10 mg/kg GP10**,** and pilocarpine+100 mg/kg glycyrrhizin as indicated. (**d**-**g**) Representative images and quantitative analysis of HE-stained CA1, CA3, and CA4 sections of hippocampus. Scale bar, 50 μm. (**h**-**k**) Representative images and quantitative analysis of Nissel-stained CA1, CA3, and CA4 sections of hippocampus collected from each group. Scale bar, 50 μm. Data are represented as mean ± SEM (n > 6). Statistical analysis was performed using unpaired Student's t-test or one-way ANOVA, ## $p < 0.01$, ### $p < 0.001$, #### $p < 0.0001$ versus Veh; * $p < 0.05$, ** $p < 0.01$, *** $p < 0.001$, **** $p < 0.0001$ versus Pilocarpine.

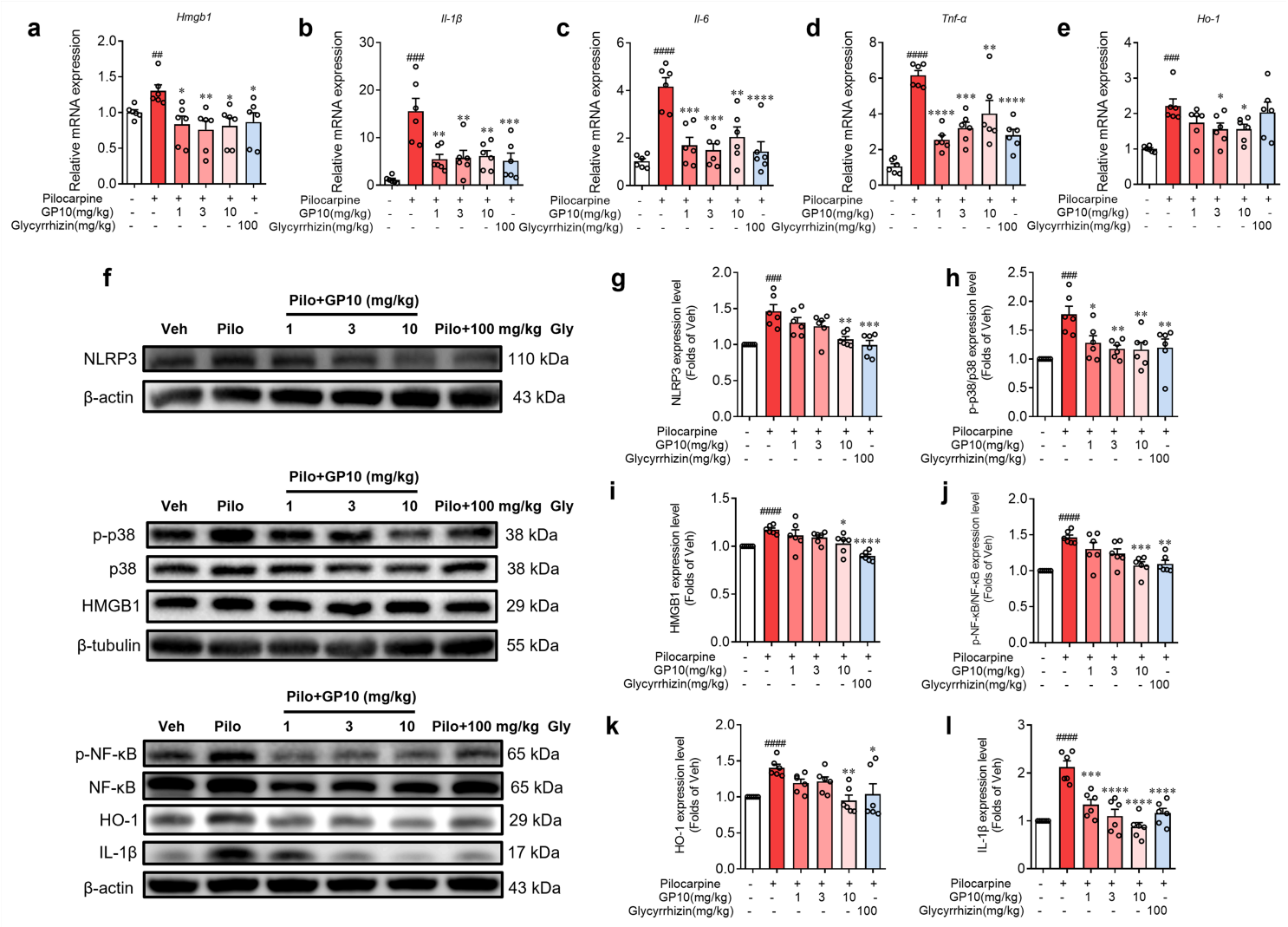


Figure 7

GP10 inhibited pilocarpine-induced inflammatory storm formation in the hippocampus. (**a**-**e**) Relative mRNA expression of *Hmgb1*, *Il-1β*, *Il-6*, *Tnf-α*, and *Ho-1*. (**f**-**l**) Western blot analysis of NLRP3, p38 phosphorylation, HMGB1, NF-κB phosphorylation, HO-1 and IL-1β. Data are represented as mean ± SEM (n = 6). Statistical analysis was performed using unpaired Student's t-test or one-way ANOVA, ## $p < 0.01$, ### $p < 0.001$, #### $p < 0.0001$ versus Veh; * $p < 0.05$, ** $p < 0.01$, *** $p < 0.001$, **** $p < 0.0001$ versus Pilocarpine.

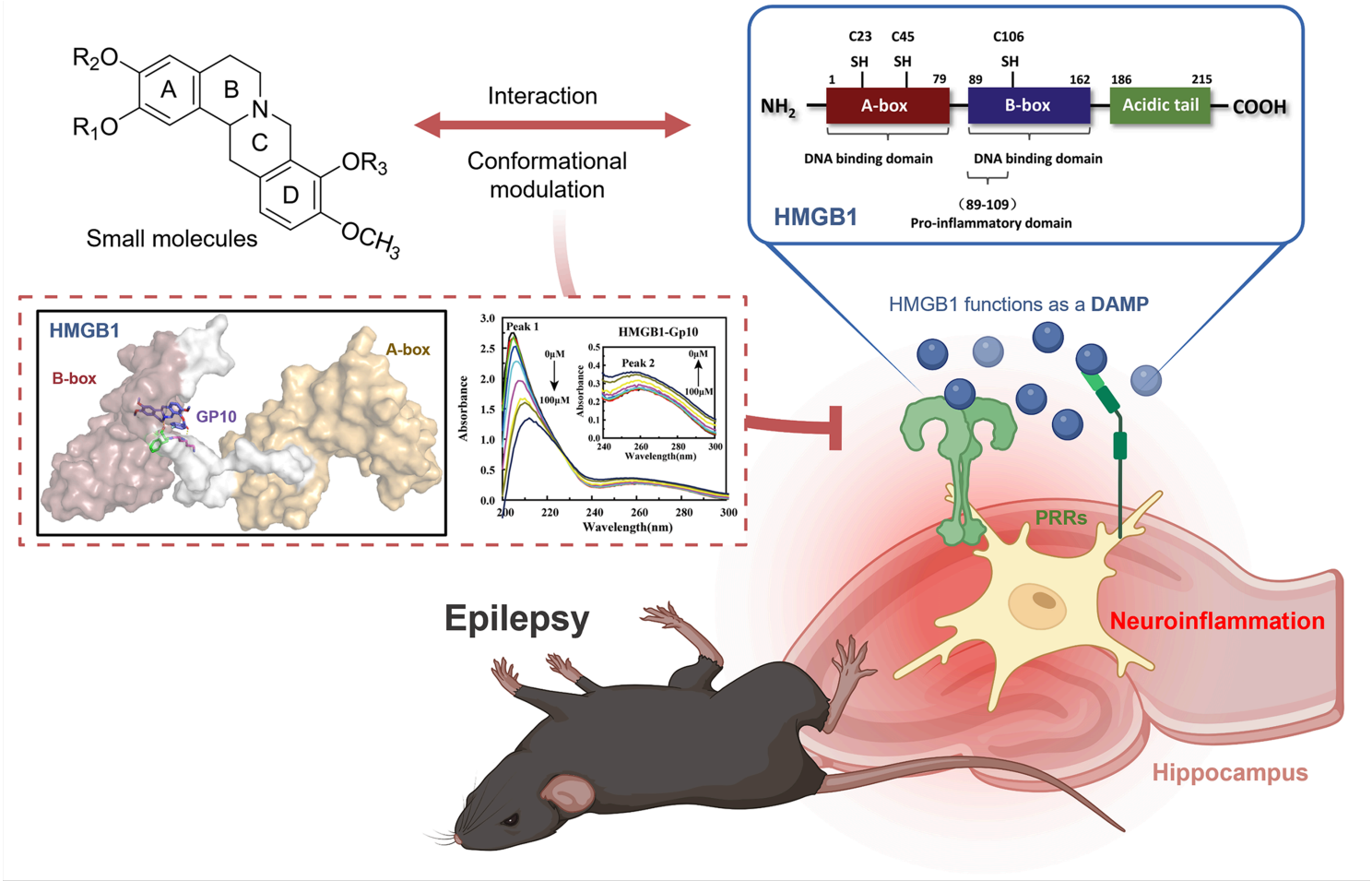


Figure 8

Graphic abstract of HMGB1 conformational intervention for epilepsy therapy. This schematic illustrates that tool small molecule bind HMGB1 to alter the conformation, thereby suppress the accumulation of HMGB1-mediated neuroinflammation as a DAMP post-seizure, and ultimately relieve epileptic symptoms. The diagram is constructed by Biorender.

Supplementary Files

This is a list of supplementary files associated with this preprint. Click to download.

- Tables.docx
- Supplementdata.docx